ACS OMEGA

http://pubs.acs.org/journal/acsodf

Article

Atmospheric-Pressure Pulsed Discharge Plasma in a Slug Flow Reactor System for the Synthesis of Gold Nanoparticles

Motoki Yamada, Wahyudiono, Siti Machmudah, Hideki Kanda, Yaping Zhao, and Motonobu Goto*

Cite This: *ACS Omega* 2020, 5, 17679−17685

Read Online

ACCESS | Metrics & More | Article Recommendations

ABSTRACT: Gold nanoparticle (AuNP) formation by applying pulsed discharge plasma in the slug flow reactor system was demonstrated. Experiments were carried out continuously at room temperature. The argon gas as a gas phase and the hydrogen tetrachloroaurate(III) tetra hydrate solution containing lysine as a liquid phase simultaneously flowed in the slug flow reactor system. The flow rates of the feed solution and argon gas were kept at 1.5 and 0.2 mL/min, respectively. To generate discharge plasma, the AC power supply with a bipolar pulsed output at 10 kV was applied. The purple color solution product was obtained, and the ultraviolet−visible (UV−vis) spectrophotometer showed that this possessed the absorption light from 510 to 550 nm associated with the existence of gold nanoparticles in each collected sample. Transmission electron microscopy (TEM) revealed that the lysine-capped AuNPs were produced in a spherical morphology and dispersed in aqueous solution products with a diameter of less than 20 nm.

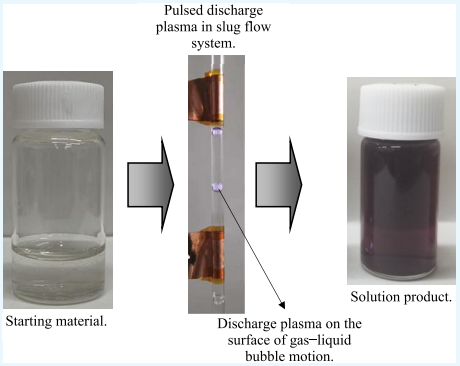

INTRODUCTION

There have been numerous studies about metal nanoparticles for their unique physicochemical properties owing to the huge surface-to-volume ratio.[1−3] And, it was well known that there are several techniques, such as chemical, physical, and biological techniques, have been employed to generate metal nanoparticles.[4−6] Physical technique (top-down), generally, focused on the size reduction of the bulk material as a starting material to generate nanoparticles. Conversely, in the chemical and biological techniques (bottom-up), nanoparticles were generated by clustering molecules or assembling atoms. Self-assembly of metal nanoparticles can be potentially used for various purposes because their spatially ordered arrangements facilitate to build complex, multifunctional, and hierarchical structures.[7,8] Among many synthetic routes for self-assembly of metal nanoparticles, bottom-up approach in the liquid media is known as realistic and cost-effective methods, wherein molecules or particles associate into functional groups under controllable thermodynamic conditions.[7,9] In this synthetic process, stabilizers are needed to control the spatial arrangements of the nanoparticles in the system if any external fields or templates as a scaffold were not given. Once ligands in stabilizers are coordinated to the surface of nanoparticles, it is considered that force balances between attractive and repulsive interactions are key to assemble nanoparticles.[10] Of course, in many cases, the use of environmentally friendly and nontoxic stabilizers is preferred.

Nonthermal plasmas in contact with the liquid media have been prepared by the bottom-up synthetic method of metal nanoparticles.[11,12] In this method, it has been reported that the metal salts in the liquid phase are reduced by electrons or hydrogen radicals initiated by pulsed discharge plasma. Therefore, advantageously, the hazardous chemicals as reducing agents are unnecessary. As the plasma discharge can be initiated more easily in a gas phase than directly in a liquid,[13] the different types of plasma generation methods at the gas−liquid interface or bubble surface in the liquid media have been reported.[11,14−16] Especially, the pulsed discharge plasma in the surface of bubbles is very effective in the radical generations,[13] so it is assumed that metal nanoparticles can be produced effectively. However, as of now, the pulsed discharge plasma in the surface of bubbles has been little considered for nanoparticles synthesis because injected gas bubbles exhibit a complex dynamic behavior in the liquid media, which made interfacial interactions between the discharged plasma in the surface of bubbles and liquid unstable.[17,18]

In this study, we developed a continuous nonthermal plasma process in a gas−liquid slug flow reactor system, where the behavior of the discharged plasma in the surface of bubbles was stably controlled with their constant intervals and flow velocity.[4,19] Thus, in our latest research, we successfully synthesized metal nanoparticles by the pulsed discharge plasma

Received: May 13, 2020
Accepted: June 26, 2020
Published: July 9, 2020

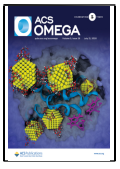

process in the slug flow reactor system.[4] In this research, we will focus on the synthesis of self-assembly of gold nanoparticles (AuNPs) in aqueous solution by the pulsed discharge plasma process in the slug flow reactor system. Among metal nanoparticles, AuNPs have many unique properties such as easy surface modification, high electrical conductivity, and controllable optical absorption spectra, which are affected by their size and shape; therefore, this nanoparticle can be used in various applications.[1,20] To promote the AuNPs self-assembly, lysine amino acid was added in the feed aqueous solution for their surface modification. A lysine molecule has two amine functional groups, which may possess the ability to bind the surface of metal nanoparticles.[7] The metal nanoparticles functionalized with amino acids are reported to self-assemble through hydrogen bond formation between carboxyl and amine groups.[21,22] As starting materials, a similar concentration of the gold ion as a precursor was dissolved in the distilled water at different pH values. The pH value of the solution is known to affect the gold ion precursor evolution to form particles.[23−25] Next, this study represents the first approach to synthesize the self-assembly of AuNPs using amino acids by pulsed discharge plasma in the slug flow reactor system.

RESULTS AND DISCUSSION

When the pulsed discharge plasma was introduced in an aqueous medium, various physical and chemical processes might occur, resulting in the active species.[4,19] These active species, such as active molecules and radicals, originated from water molecules via dissociation reaction. Also, it has been known that the hydroxyl radical and hydrogen peroxide were recognized as the major active species participating in the chemical reaction including the AuNPs generation during pulsed discharge plasma application. Hence, it could be said that the major reactions during pulsed discharge plasma applications in water are hydrogen peroxide generation and water dissociation.[19,26] Of course, a positive effect was also obtained with the bubbles injection during the process where the bubbles may help the discharge plasma generation with the low energy yields.[19,26,27] The formation of AuNPs was started by the interaction between the Au^{3+} ions and the active species produced from water dissociation.[23−25] This reduction reaction resulted in Au^0 metal particles in aqueous solution. At the same time, the active species also attack the lysine molecule through hydrogen abstraction from the α-carbon of the −CO−NH−peptide bonds, resulting in the lysine reactive sites, and it was then followed by the interaction between these active sites of lysine and the Au^0 metal particles.[6,28] Hence, by applying the pulsed discharge plasma process in slug flow reactor system as mentioned in the Material and Method-Section, the aqueous solution containing AuNPs can be continuously produced. Note that the AuNP amount in the collected sample was not determined. Several parameters, i.e., solution conductivity, pulse width, pulse frequency, and applied voltages, which can affect the AuNP formation process during pulsed discharge plasma application, were also not observed. The simple plausible reaction mechanism of AuNPs was expressed in eqs 1−4, where reactions 3 and 4 occur in the acid conditions (pH 3.5) and the base conditions (pH 9.5 and 11.5), respectively[23−25]

$$H_2O \rightarrow H^{\bullet} + OH^{\bullet} \quad (1)$$

$$2H_2O \rightarrow H_2O_2 + H_2 \quad (2)$$

$$AuCl_4^- + 3H^{\bullet} \rightarrow 3HCl + Au^0 + Cl^- \quad (3)$$

$$Au(OH)_4^- + 3H^{\bullet} \rightarrow 3H_2O + Au^0 + OH^- \quad (4)$$

Figures 1 and 2 show typical photographs and ultraviolet−visible (UV−vis) spectra of lysine-capped AuNPs liquid products after pulsed discharge plasma treatment at different pH values. The purple color of liquid products is due to the AuNPs characteristics of surface plasmon resonance.[20,29] This implies that the AuNPs dispersed stably in aqueous solution products. It is also known that the peak optical absorption in AuNPs ranges from 510 to 550 nm in wavelength, and the spectral intensity depends on the number, shape, and dispersity of the particles.[20,30,31]

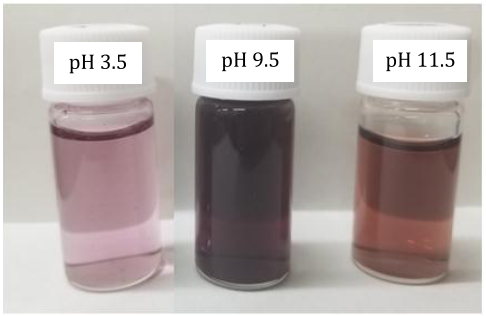

Figure 1. Typical photographs of AuNPs liquid products prepared at various pH values from the slug flow reactor system.

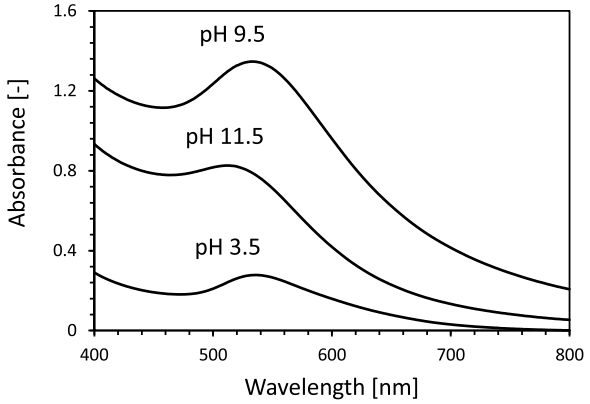

Figure 2. UV−vis spectra of AuNP liquid products prepared at various pH values from the slug flow reactor system.

In this experiment, although the purple colors of the liquid products were found at all pH conditions, the liquid product at pH 9.5 possessed the stronger purple color and the higher optical absorption than those produced at any other pH conditions. This indicates that the difference in the pH value resulted in a structural or organizational change in AuNPs. When appearances of the liquid products were compared between acid (pH 3.5) and base (pH 11.5) conditions, the colors were slightly different: the purple color was found in an acid condition, while the liquid product in base condition had red-purple color. This difference was also found by the UV−vis absorption peak spectra, where the strong absorption peak intensity at 535 nm was found in acid condition, while in base condition, the strong absorption peak intensity occurs at 511 nm. It is well known that the increase in gold nanoparticle size may result in a red shift of peak absorption spectra.[20]

https://dx.doi.org/10.1021/acsomega.0c02217
ACS Omega 2020, 5, 17679−17685

Therefore, in this experiment, it could be said that the larger size of gold nanoparticles might be produced in acid conditions compared to those in base conditions.

Next, the AuNP physical properties such as dispersity, shape, and size were observed using a transmission electron microscopy (TEM) device. Figure 3 shows the representative

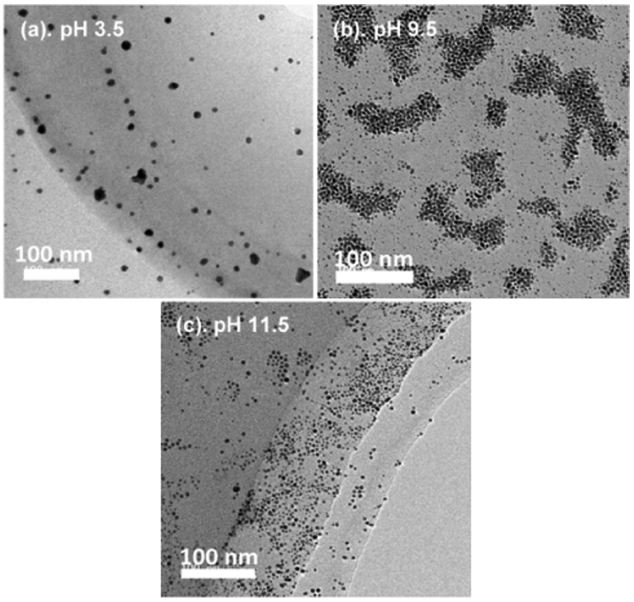

Figure 3. TEM images of lysine-capped AuNPs products from the slug flow reactor system at various pH conditions.

TEM images of lysine-capped AuNPs produced by applying pulsed discharge plasma in the slug flow reactor system at each pH condition. At all pH conditions, spherical AuNPs were observed and obviously dispersed in aqueous solution products. This indicated that self-assembled AuNPs might occur especially at pH 9.5 condition.[32−34] As a result, the strongest optical absorption was found at this pH condition. Selvakannan et al.[32] reported that AuNP assembly was successfully synthesized with lysine at isoelectric point (pI) in aqueous solution by gold ion reduction using sodium borohydride, and they explained the mechanism of gold nanoparticles assembly. At first, one amino group ($-NH_2$) in lysine bound to the surface of AuNPs. Next, the terminal amino group and a carboxyl group (−COOH) formed a hydrogen bond with functional groups of lysine molecules bound to the surface of the neighboring AuNPs. Considering this mechanism, the layer of lysine molecules might be formed between the neighboring particles, which had an interparticle distance of around 1.5−2.0 nm (see Figure 4).[35,36] This image (Figure 4) also confirmed that the self-assembly of AuNPs in this study was successfully carried out mainly at pH 9.5, near the pI of lysine amino acid. Note, the pI of lysine amino acid is around 9.74. Next, according to the TEM images (Figure 3), the particle size of lysine-capped AuNPs was determined using ImageJ software. At least 300 diverse lysine-capped AuNPs were randomly selected from each image in Figure 3.

As shown in Figure 5, different sizes of lysine-capped AuNPs in each population were found in each condition. Probably, this is attributed to the fact that the total electric charge of the lysine is not equally balanced: the lysine molecules are negatively charged at high pH conditions, while positively charged at low pH. This might cause the electrostatic repulsion

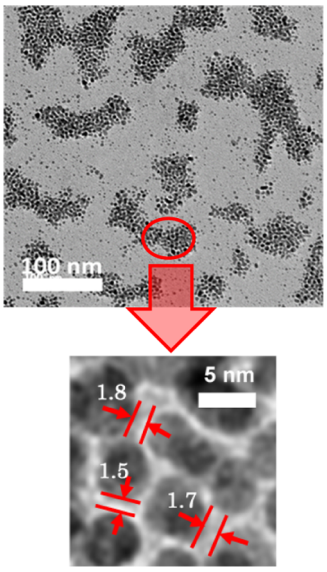

Figure 4. Interparticle distance calculated from high-magnification TEM image in assembly AuNPs at pH 9.5 condition.

among the charged functional groups of lysine bound to the surface of AuNPs, resulting in the AuNPs simply dispersed without forming the assembled structure. As a result, the different sizes of particles were generated.[32−34] At lower pH (pH 3.5), although the dissociation of the carboxylic group does not occur, and hence the interaction of the carboxyl group could be suppressed, however, the amine group interaction was still activated by the zwitterionic species. This will promote the aggregation of lysine-capped AuNPs, resulting in a larger diameter. At higher pH (pH 9.5 and 11.5), the dissociation of the carboxyl group occurred, thus it was expected to obstruct the cross-linking via the binding of the gold particles and amine group.[32−34] Accordingly, as shown in Figure 5, the smaller diameter of lysine-capped AuNPs was obtained when the experiments were performed at higher pH values. In addition, in agreement with the result mentioned in Figure 2, where the peak absorption spectra of a liquid product containing gold nanoparticle at acid condition underwent a red shift in absorption spectra, this also confirmed that the relatively larger AuNPs were obtained when the pulsed discharge plasma process in the slug flow reactor system was performed at an acid condition.

Table 1 summarized the values of ζ-potentials and average sizes of the AuNPs at different pH conditions. It is already known that ζ-potentials of metal nanoparticles had a positive value at low pH conditions due to a large amount of H^+ ions in aqueous media, but it became negative at high pH conditions. Hence, as described in this table, the surface of AuNPs had positive charges at an acid condition while they possessed negative charges at a base condition.[37,38] At acid conditions, the electrostatic interactions between the lysine molecules and the AuNPs via their surface might be suppressed because both had a positive charge. As a result, the generation of lysine-capped AuNPs might proceed slowly, while the growth of AuNP was dominant.[38] Figure 6 shows the thermogravimetric analyzer (TGA) plots recorded from the lysine-capped AuNPs powder and original lysine. Prior to TGA analysis, the liquid products containing lysine-capped AuNPs were treated by freeze-drying (Eyela FDU-1200, Rikakikai Co. Ltd., Tokyo, Japan) to release water content. In this treatment, the water in

https://dx.doi.org/10.1021/acsomega.0c02217
ACS Omega 2020, 5, 17679−17685

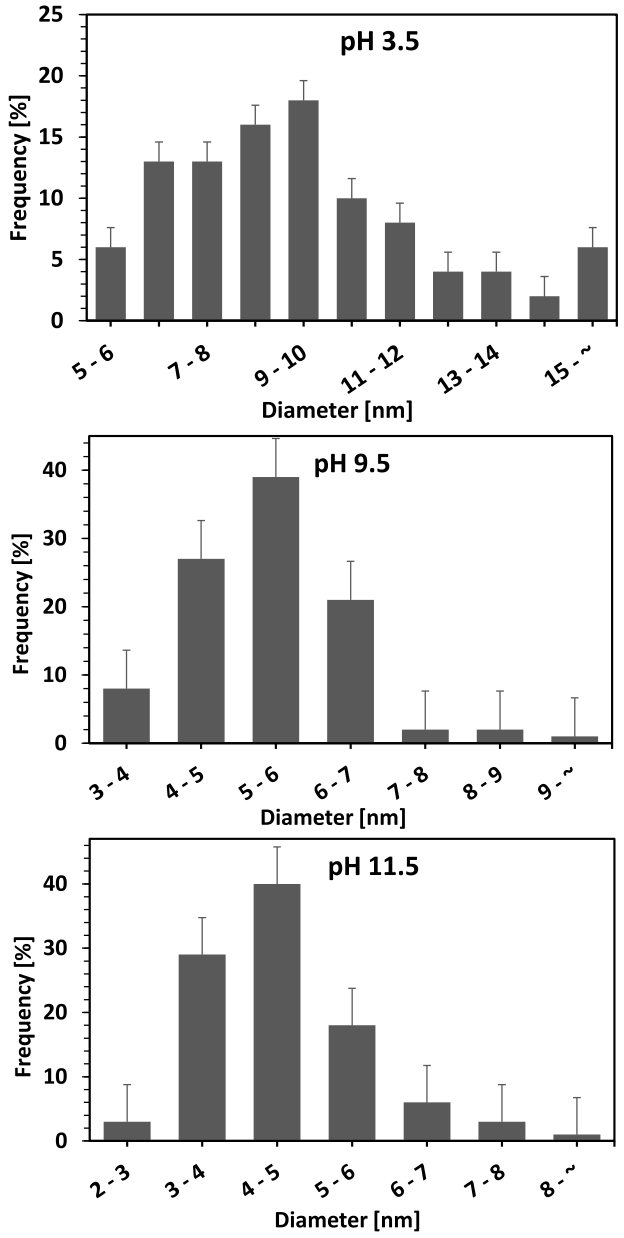

Figure 5. Particle size distributions of lysine-capped AuNPs products from the slug flow reactor system at various pH conditions.

Table 1. ζ-Potential and Average Size of AuNPs Produced by This Method at Various pH Conditions

	pH		
parameter	3.5	9.5	11.5
ζ-potential (mV)	+27.0 + 8.32	−31.1 + 8.01	−32.1 + 8.14
average particle size (nm)	9.8 + 3.20	5.4 + 1.02	4.5 + 1.02

the collected products is released via the sublimation process. Next, the lysine-capped AuNP powder was weighed (approximately 10 mg) in a platinum open pan, and the weight loss was monitored in the temperature ranging from 30 °C (room temperature) to 1000 °C. As shown in Figure 6, the lysine-capped AuNPs powder underwent weight losses in the temperature range of 70−560 °C (about 40% weight loss) and 760−930 °C (additional 30% weight loss). The thermal

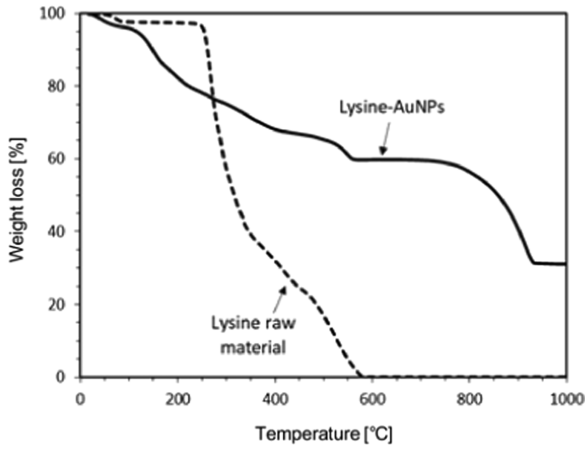

Figure 6. TGA curves of lysine raw material and lysine-capped AuNP powder.

degradation of the lysine-capped AuNPs powder seems to complete at around 930 °C. Hence, there was no further weight loss above this temperature. On the other hand, the lysine raw material underwent a steep weight loss in the temperature range of 250−580 °C, and it was continued to a relatively constant weight period. It indicated that the major loss of weight of lysine occurs in these range temperatures (250−580 °C). The plot of the lysine-capped AuNPs powder also seems to have a peculiar weight loss in the temperature range of 70−560 °C. Considering the plot of lysine raw material, it might be due to the evolution of water and volatile matter from the lysine-capped AuNPs.

In addition, the decomposition of lysine molecules also occurs in these ranges of temperature. With increasing temperature, the other weight loss of the lysine-capped AuNP powder was observed in the temperature range of 760−930 °C. It indicated that the strongly bound lysine molecules on the AuNP surface were detached and decomposed in these temperature ranges. This curve also pointed out that the interaction of lysine molecule AuNPs resulted in more stable lysine molecules.[32,39,40]

To prove the existence of the surface-bound lysine molecules on the AuNPs, the lysine-capped AuNPs and the original lysine powders were characterized by infrared spectroscopy (Fourier transform infrared, FTIR) in the 4000−400 cm^{-1} wavenumber. The spectrum of the protein−peptide group exhibits some different bands,[41,42] such as amide A (∼3300 cm^{-1}), amide B (∼3100 cm^{-1}), amide I (∼1650 cm^{-1}), amide II (∼1550 cm^{-1}), amide III (∼1300 cm^{-1}), amide IV (∼735 cm^{-1}), amide V (∼635 cm^{-1}), amide VI (∼600 cm^{-1}), and amide VII (∼200 cm^{-1}). Figure 7 illustrates the FTIR spectra of the original lysine and the lysine-capped AuNPs powders. As informed before that the self-assembly of metal nanoparticles with amino acids occurs via the formation of the hydrogen bond between carboxyl and amine groups.[21,22] Accordingly, as shown in Figure 7, the peaks intensity in the 1622 and 3122 cm^{-1} regions corresponding to C═O stretching (amide I group) and N−H stretching (amide A group), which are found in original lysine spectra, disappeared or became weaker after treatment by applying pulsed discharge plasma to synthesize the self-assembly of AuNPs with lysine. This indicated that the interaction between lysine molecules and AuNPs occurs during the application of pulsed discharge plasma in the slug flow reactor system. This result also may

https://dx.doi.org/10.1021/acsomega.0c02217
ACS Omega 2020, 5, 17679−17685

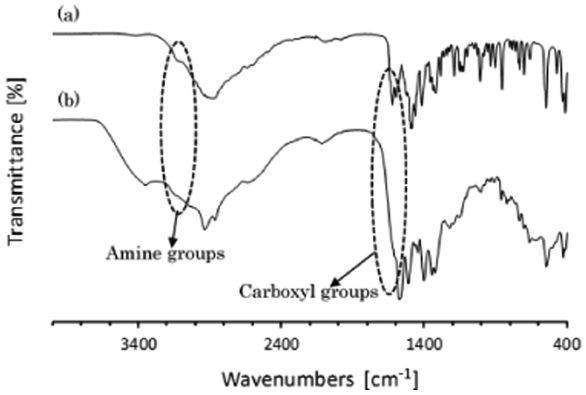

Figure 7. FTIR spectra of lysine raw material (a) and lysine-capped AuNPs powder (b).

confirm that the carboxyl group and the amine group of lysine molecules attached and bound on the gold nanoparticles after pulsed discharge plasma treatment.[43,44]

CONCLUSIONS

Self-assembly of AuNPs using lysine was successfully performed by applying a pulsed discharge plasma in the slug flow reactor system at room temperature. As a gas phase and a liquid phase, the argon gas and the $HAuCl_4{\cdot}4H_2O$ solution containing lysine flowed simultaneously in the slug flow reactor system. After their flow was stable, the AC power supply with a bipolar pulsed output (10 kV) was introduced to generate a pulsed discharge plasma. The UV−vis spectrophotometer showed that the solution products possessed the absorption light from 510 to 550 nm associated with the gold nanoparticle formation in each collected sample. The TEM images revealed that the lysine-capped AuNPs had spherical morphology and dispersed in solution products. Further analysis (FTIR) indicated that the lysine molecules attached and bound on the AuNPs through the formation of the hydrogen bond between carboxyl and amine groups after pulsed discharge plasma application. It could be said that the pulsed discharge plasma in this slug flow reactor system could supply the active species, which can promote the reduction reaction of the gold ion into the neutral atom to form particles. Next, this experimental result can be used to update the information for the generation of metal nanoparticles from metal ion precursors in the slug flow reactor system by applying pulsed discharge plasma.

MATERIALS AND METHOD

Materials. The hydrogen tetrachloroaurate(III) tetra hydrate ($HAuCl_4{\cdot}4H_2O$), L(+)-lysine hydrochloride (H_2N-$(CH_2)4CH(NH_2)COOH{\cdot}HCl$), and sodium hydroxide (NaOH, pellet) as feed materials were bought from FUJIFILM Wako Pure Chemical Corporation, Osaka, Japan. Distilled water (CAS. No. 7732-18-5; Product No. 049-16787) as the liquid media was also bought from FUJIFILM Wako Pure Chemical Corporation. Note, all materials were used as received. Argon (Ar) with a purity greater than 99.99% were purchased from Tomoe Shokai Co, Ltd., Tokyo, Japan. The feed solution was prepared with a mixture of $HAuCl_4{\cdot}4H_2O$ (2.0 mmol/L) and lysine hydrochloride (5.0 mmol/L). They were dissolved in distilled water. As the initial pH value of the prepared solution was 3.5. The higher pH of the solutions was adjusted by the addition of NaOH. The feed solutions were then stored in a desiccator at room temperature.

Experimental Setup and Procedure. Figure 8 shows the apparatus scheme of the nonthermal plasma with a pulsed

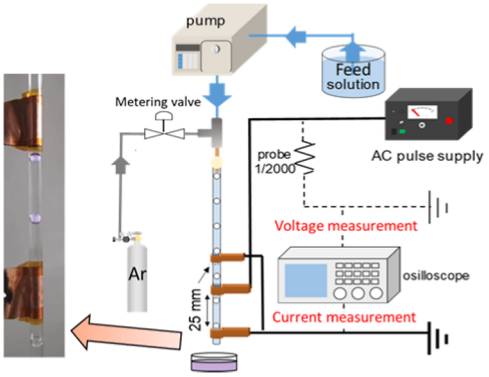

Figure 8. Apparatus scheme of discharge plasma in the slug flow reactor system.

discharge in a slug flow reactor system. The apparatus consisted of a glass capillary tube (2.0 mm i.d.), liquid pump (HPLC, LC−10AD, Shimadzu Co., Japan), gas flow meter (RK-1250, Kofloc Instruments Inc., Japan), and AC power supply (TE-HVP1510K300−NP, Tamaoki Electronics Co. Ltd., Japan). The feed solution was degassed for about 10 min to remove the dissolved air, and the argon gas was flowed in the slug flow reactor system to purge the air before starting the experiments. To generate the gas−liquid slug flow in the glass capillary, the feed solution and argon gas were flowed simultaneously from different directions and mixed via union Tee junction (SS-200-3, Swagelok). This union Tee junction was connected to the upper part of the glass capillary. By controlling their flow rates, the gas−liquid slug flow with the equal interval of bubbles was formed in the glass capillary.

In this experiment, flow rates of the feed solution and argon gas were kept at 1.5 and 0.2 mL/min, respectively, using a HPLC pump and a gas flow meter device. The intervals of bubbles in the glass capillary were around 10 ± 2 mm. As a high-voltage electrode, a 1 cm wide copper sheet was prepared and attached on the outside surface of the glass capillary. In the same way, two ground electrodes were attached to the glass capillary at the top and the bottom sides from the high-voltage electrode. Therefore, there is no direct contact between the argon gas or the aqueous solution and the copper sheet electrodes during experiments, accordingly, the contamination of the product can be avoided. Conversely, the contamination on the final products may occur when metal rods, except a gold rod, were employed as electrodes to generate discharge plasma (arc discharge plasma).[6,18] The distance between the copper sheets as high-voltage electrodes and those as ground electrodes was about 25 mm. After the flowing bubbles in the glass capillary were stable, electrical discharge from a power supply with a bipolar pulsed output was introduced into the slug flow reactor system via copper sheets to generate plasma. The 10 kV output voltage at 10 kHz repetition was transferred to the moving bubbles in the slug flow reactor system. No power variation was investigated in this experiment. A digital oscilloscope (TDS2024C, Tektronix Inc.) that was equipped and connected to a high-voltage probe and a current transformer was used to monitor the applied voltage and

https://dx.doi.org/10.1021/acsomega.0c02217
ACS Omega 2020, 5, 17679−17685

current during the pulsed discharge plasma application. The liquid products containing lysine-capped AuNPs were collected directly from the glass capillary.

Analytical Methods. To understand the AuNP generation, the liquid products were analyzed by ultraviolet−visible (UV−vis) spectrophotometer (V-550, JASCO Corporation, Japan) ranging from 400 to 800 nm. The ζ-potentials (effective surface charge) of the AuNPs in aqueous solution were measured with Zetasizer (Nano ZS, Malvern Panalytical Ltd., U.K.). Drops of lysine-capped AuNP liquid products were placed on the carbon-coated copper grids and characterized by transmission electron microscopy (TEM, JEM-2100Plus, Japan Electronic Co., Ltd). The sizes of AuNPs were also measured from the TEM images using image analysis of ImageJ software. Before TEM analysis, the carbon-coated copper grids containing AuNPs were placed and dried immediately in the desiccator overnight at ambient conditions to minimize the AuNP aggregation.[45] The thermal behavior of lysine-capped AuNP powders and a lysine raw material were characterized by a thermogravimetric analyzer (TGA, Thermo Plus TG8120, Rigaku Corporation, Japan) at a heating rate of 5 °C/min in a nitrogen atmosphere. A lysine raw material and lysine-capped AuNP powders were also characterized by a Fourier transform infrared (FTIR) spectrophotometer (Spectrum Two, PerkinElmer Ltd., England).

AUTHOR INFORMATION

Corresponding Author

Motonobu Goto − *Department of Materials Process Engineering, Nagoya University, Nagoya 464-8603, Japan;* orcid.org/0000-0003-3219-5028; Phone: +81-52-789-3992; Email: goto.motonobu@material.nagoya-u.ac.jp; Fax: +81-52-789-3989

Authors

Motoki Yamada − *Department of Materials Process Engineering, Nagoya University, Nagoya 464-8603, Japan*

Wahyudiono − *Department of Materials Process Engineering, Nagoya University, Nagoya 464-8603, Japan;* orcid.org/0000-0003-0339-1740

Siti Machmudah − *Department of Chemical Engineering, Sepuluh Nopember Institute of Technology, Surabaya 60111, Indonesia;* orcid.org/0000-0002-4927-0402

Hideki Kanda − *Department of Materials Process Engineering, Nagoya University, Nagoya 464-8603, Japan*

Yaping Zhao − *School of Chemistry & Chemical Engineering, Shanghai Jiao Tong University, Shanghai 200240, China;* orcid.org/0000-0001-5682-3370

Complete contact information is available at: https://pubs.acs.org/10.1021/acsomega.0c02217

Author Contributions

All authors have given approval to the final version of the manuscript.

Notes

The authors declare no competing financial interest.

ACKNOWLEDGMENTS

This work was supported by JSPS KAKENHI Grant Number JP20H02515 and JST SICORP Grant Number JPMJSC18H1, Japan.

ABBREVIATIONS USED

AuNPs:gold nanoparticles; UV−vis:ultraviolet−visible; TEM:-transmission electron microscopy; TGA:thermogravimetric analyzer; pI:isoelectric point; FTIR:Fourier transform infrared spectroscopy

REFERENCES

(1) Duhan, J. S.; Kumar, R.; Kumar, N.; Kaur, P.; Nehra, K.; Duhan, S. Nanotechnology: The new perspective in precision agriculture. *Biotechnol. Rep.* **2017**, *15*, 11−23.

(2) Chen, Y.; Fan, Z.; Zhang, Z.; Niu, W.; Li, C.; Yang, N.; Chen, B.; Zhang, H. Two-Dimensional Metal Nanomaterials: Synthesis, Properties, and Applications. *Chem. Rev.* **2018**, *118*, 6409−6455.

(3) Yang, J.; Hou, B.; Wang, J.; Tian, B.; Bi, J.; Wang, N.; Li, X.; Huang, X. Nanomaterials for the Removal of Heavy Metals from Wastewater. *Nanomater* **2019**, *9*, No. 424.

(4) Yamada, M.; Takahashi, S.; Wahyudiono; Takada, N.; Kanda, H.; Goto, M. Synthesis of silver nanoparticles by atmospheric-pressure pulsed discharge plasma in a slug flow system. *Jpn. J. Appl. Phys.* **2018**, *58*, No. 016001.

(5) Bilal, M.; Iqbal, H. M. N. Chemical, physical, and biological coordination: An interplay between materials and enzymes as potential platforms for immobilization. *Coord. Chem. Rev.* **2019**, *388*, 1−23.

(6) Wahyudiono; Kondo, H.; Yamada, M.; Takada, N.; Machmudah, S.; Kanda, H.; Goto, M. DC-Plasma over Aqueous Solution for the Synthesis of Titanium Dioxide Nanoparticles under Pressurized Argon. *ACS Omega* **2020**, *5*, 5443−5451.

(7) Thiruvengadathan, R.; Korampally, V.; Ghosh, A.; Chanda, N.; Gangopadhyay, K.; Gangopadhyay, S. Nanomaterial processing using self-assembly-bottom-up chemical and biological approaches. *Rep. Prog. Phys.* **2013**, *76*, No. 066501.

(8) Boles, M. A.; Engel, M.; Talapin, D. V. Self-Assembly of Colloidal Nanocrystals: From Intricate Structures to Functional Materials. *Chem. Rev.* **2016**, *116*, 11220−11289.

(9) Kim, J. H.; Jin, H. M.; Yang, G. G.; Han, K. H.; Yun, T.; Shin, J. Y.; Jeong, S.-J.; Kim, S. O. Smart Nanostructured Materials based on Self-Assembly of Block Copolymers. *Adv. Funct. Mater.* **2020**, *30*, No. 1902049.

(10) Lee, Y. S. *Self-Assembly and Nanotechnology Systems: Design, Characterization, and Applications*; John Wiley & Sons, Inc.: New Jersey, USA, 2011; p 4.

(11) Kaneko, T.; Baba, K.; Harada, T.; Hatakeyama, R. Novel Gas-Liquid Interfacial Plasmas for Synthesis of Metal Nanoparticles. *Plasma Processes Polym.* **2009**, *6*, 713−718.

(12) Wei, Z.; Liu, C.-j. Synthesis of monodisperse gold nanoparticles in ionic liquid by applying room temperature plasma. *Mater. Lett.* **2011**, *65*, 353−355.

(13) Nishiyama, H.; Nagai, R.; Niinuma, K.; Takana, H. Characterization of DBD Multiple Bubble Jets for Methylene Blue Decolorization. *J. Fluid Sci. Technol.* **2013**, *8*, 65−74.

(14) Sato, M.; Ohgiyama, T.; Clements, J. S. Formation of chemical species and their effects on microorganisms using a pulsed high-voltage discharge in water. *IEEE Trans. Ind. Appl.* **1996**, *32*, 106−112.

(15) Bruggeman, P.; Degroote, J.; Vierendeels, J.; Leys, C. DC-excited discharges in vapour bubbles in capillaries. *Plasma Sources Sci. Technol.* **2008**, *17*, No. 025008.

(16) Lee, S. W.; Liang, D.; Gao, X. P. A.; Sankaran, R. M. Direct Writing of Metal Nanoparticles by Localized Plasma Electrochemical Reduction of Metal Cations in Polymer Films. *Adv. Funct. Mater.* **2011**, *21*, 2155−2161.

(17) Bruggeman, P.; Leys, C. Non-thermal plasmas in and in contact with liquids. *J. Phys. D: Appl. Phys.* **2009**, *42*, No. 053001.

(18) Chen, Q.; Li, J.; Li, Y. A review of plasma-liquid interactions for nanomaterial synthesis. *J. Phys. D: Appl. Phys.* **2015**, *48*, No. 424005.

(19) Wahyudiono; Mano, K.; Hayashi, Y.; Yamada, M.; Takahashi, S.; Takada, N.; Kanda, H.; Goto, M. Atmospheric-pressure pulsed

https://dx.doi.org/10.1021/acsomega.0c02217
ACS Omega 2020, 5, 17679−17685

discharge plasma in capillary slug flow system for dye decomposition. *Chem. Eng. Process Process Intensif.* **2019**, *135*, 133−140.
(20) Jain, P. K.; Lee, K. S.; El-Sayed, I. H.; El-Sayed, M. A. Calculated Absorption and Scattering Properties of Gold Nanoparticles of Different Size, Shape, and Composition: Applications in Biological Imaging and Biomedicine. *J. Phys. Chem. B.* **2006**, *110*, 7238−7248.
(21) Johnson, S. R.; Evans, S. D.; Brydson, R. Influence of a Terminal Functionality on the Physical Properties of Surfactant-Stabilized Gold Nanoparticles. *Langmuir* **1998**, *14*, 6639−6647.
(22) Zong, J.; Cobb, S. L.; Cameron, N. R. Peptide-functionalized gold nanoparticles: versatile biomaterials for diagnostic and therapeutic applications. *Biomater. Sci.* **2017**, *5*, 872−886.
(23) Bratescu, M. A.; Cho, S.-P.; Takai, O.; Saito, N. Size-controlled gold nanoparticles synthesized in solution plasma. *J. Phys. Chem. C* **2011**, *115*, 24569−24576.
(24) Moore Tibbetts, K.; Tangeysh, B.; Odhner, J. H.; Levis, R. J. Elucidating strong field photochemical reduction mechanisms of aqueous [AuCl4]?: Kinetics of multiphoton photolysis and radical-mediated reduction. *J. Phys. Chem. A* **2016**, *120*, 3562−3569.
(25) Xie, P.; Qi, Y.; Wang, R.; Wu, J.; Li, X. Aqueous Gold Nanoparticles Generated by AC and Pulse-Power-Driven Plasma Jet. *Nanomaterials* **2019**, *9*, No. 1488.
(26) Locke, B. R.; Shih, K.-Y. Review of the methods to form hydrogen peroxide in electrical discharge plasma with liquid water. *Plasma Sources Sci. Technol.* **2011**, *20*, No. 034006.
(27) Hamdan, A.; Cha, M. S. The effects of gaseous bubble composition and gap distance on the characteristics of nanosecond discharges in distilled water. *J. Phys. D: Appl. Phys.* **2016**, *49*, No. 245203.
(28) Parvulescu, V. I.; Magureanu, M.; Lukes, P. *Plasma Chemistry and Catalysis in Gases and Liquids*; Wiley-VCH Verlag & Co. KGaA: Weinheim, Germany, 2012; p 185.
(29) Wang, S.; Zhang, H.; Li, W.; Birech, Z.; Ma, L.; Li, D.; Li, S.; Wang, L.; Shang, J.; Hu, J. A multi-channel localized surface plasmon resonance system for absorption metric determination of abscisic acid by using gold nanoparticles functionalized with a polyadenine-tailed aptamer. *Microchim. Acta* **2020**, *187*, No. 20.
(30) Wright, A.; Gabaldon, J.; Burckel, D. B.; Jiang, Y.-B.; Tian, Z. R.; Liu, J.; Jeffrey Brinker, C.; Fan, H. Hierarchically organized nanoparticle mesostructure arrays formed through hydrothermal self-assembly. *Chem. Mater.* **2006**, *18*, 3034−3038.
(31) Ramírez-García, G.; Honorato-Colin, M. Á.; De la Rosa, E.; López-Luke, T.; Panikar, S. S.; de Jesús Ibarra-Sánchez, J.; Piazza, V. Theranostic nanocomplex of gold-decorated upconversion nanoparticles for optical imaging and temperature-controlled photothermal therapy. *J. Photochem. Photobiol., A.* **2019**, *384*, No. 112053.
(32) Selvakannan, P. R.; Mandal, S.; Phadtare, S.; Pasricha, R.; Sastry, M. Capping of Gold Nanoparticles by the Amino Acid Lysine Renders Them Water-Dispersible. *Langmuir* **2003**, *19*, 3545−3549.
(33) Zare, D.; Akbarzadeh, A.; Bararpour, N. Synthesis and Functionalization of Gold Nanoparticles by Using of Poly Functional Amino Acids. *Int. J. Nanosci. Nanotechnol.* **2010**, *6*, 223−230.
(34) Shu, M.; He, F.; Li, Z.; Zhu, X.; Ma, Y.; Zhou, Z.; Yang, Z.; Gao, F.; Zeng, M. Biosynthesis and Antibacterial Activity of Silver Nanoparticles Using Yeast Extract as Reducing and Capping Agents. *Nanoscale Res. Lett.* **2020**, *15*, No. 14.
(35) Song, C.; Blaber, M. G.; Zhao, G.; Zhang, P.; Fry, H. C.; Schatz, G. C.; Rosi, N. L. Tailorable plasmonic circular dichroism properties of helical nanoparticle superstructures. *Nano Lett.* **2013**, *13*, 3256−3261.
(36) Esashika, K.; Ishii, R.; Tokihiro, S.; Saiki, T. Simple and rapid method for homogeneous dimer formation of gold nanoparticles in a bulk suspension based on van der Waals interactions between alkyl chains. *Opt. Mater. Express* **2019**, *9*, 1667−1677.
(37) Dougherty, G. M.; Rose, K. A.; Tok, J. B.-H.; Pannu, S. S.; Chuang, F. Y. S.; Sha, M. Y.; Chakarova, G.; Penn, S. G. The zeta potential of surface-functionalized metallic nanorod particles in aqueous solution. *Electrophoresis* **2008**, *29*, 1131−1139.
(38) El-Trass, A.; ElShamy, H.; El-Mehasseb, I.; El-Kemary, M. CuO nanoparticles: Synthesis, characterization, optical properties and interaction with amino acids. *Appl. Surf. Sci.* **2012**, *258*, 2997−3001.
(39) Zarabi, M. F.; Arshadi, N.; Farhangi, A.; Akbarzadeh, A. Preparation and Characterization of Gold Nanoparticles with Amino Acids, Examination of Their Stability. *Indian J. Clin. Biochem.* **2014**, *29*, 306−314.
(40) Zheng, Y.; Cheng, F.; He, W. Epoxy-Amine microgels-mediated green preparation of gold nanoparticles. *Colloids Surf., A* **2019**, *575*, 94−101.
(41) Sabbatini, S.; Conti, C.; Orilisi, G.; Giorgini, E. Infrared spectroscopy as a new tool for studying single living cells: is there a niche? *Biomed. Spectrosc. Imaging* **2017**, *6*, 85−99.
(42) Usoltsev, D.; Sitnikova, V.; Kajava, A.; Uspenskaya, M. Systematic FTIR Spectroscopy Study of the Secondary Structure Changes in Human Serum Albumin under Various Denaturation Conditions. *Biomolecules* **2019**, *9*, No. 359.
(43) Ashjari, M.; Dehfuly, S.; Fatehi, D.; Shabani, R.; Koruji, M. Efficient functionalization of gold nanoparticles using cysteine conjugated protoporphyrin IX for singlet oxygen production in vitro. *RSC Adv.* **2015**, *5*, 104621−104628.
(44) Aldewachi, H.; Woodroofe, N.; Gardiner, P. Study of the stability of functionalized gold nanoparticles for the colorimetric detection of dipeptidyl peptidase IV. *Appl. Sci.* **2018**, *8*, No. 2589.
(45) Neil, C. W.; Ray, J. R.; Lee, B.; Jun, Y.-S. Fractal aggregation and disaggregation of newly formed iron (III)(hydr) oxide nanoparticles in the presence of natural organic matter and arsenic. *Environ. Sci.: Nano* **2016**, *3*, 647−656.

https://dx.doi.org/10.1021/acsomega.0c02217
ACS Omega 2020, 5, 17679−17685